Germanium:gallium photoconductors for far infrared heterodyne detection

I. S. Park, E. E. Haller, E. N. Grossman, and Dan M. Watson

Highly compensated Ge:Ga photoconductors have been fabricated and evaluated for high bandwidth heterodyne detection. Bandwidths up to 60 MHz have been obtained with corresponding current responsivity of 0.01 A/W.

I. Introduction

Extrinsic germanium photoconductors have long been the premier devices for high sensitivity direct detection in the 20–200-μm wavelength region.[1,2] Quantum efficiencies over 40% and noise equivalent powers (NEPs) of $<10^{-16}$ W Hz$^{-1/2}$ have been achieved. Although well characterized in terms of responsivity and direct detection NEP, the high speed (comparable with the inverse recombination time) properties of photoconductive detectors have not been studied in detail. Recently, however, considerable interest has arisen among astronomers, plasma physicists, and others in extending the techniques of high sensitivity millimeter and submillimeter heterodyne detection to the far infrared.[3,4] In response, we have performed an investigation of the suitability of extrinsic photoconductors as heterodyne mixers in this wavelength region. In particular, the dependence of detector bandwidth on the concentration of compensating impurities is a critical issue in the optimization of heterodyne performance and has hitherto not been studied in detail for shallow impurities.

Extrinsic photoconductors are used in many applications as square-law devices: their signal current output is proportional to the radiation power input, i.e., to the square of the incident field amplitudes.[5] The signal can be mixed with a strong continuous wave (cw) local oscillator (LO) field at a nearby frequency, leading to new frequencies: the sum and difference of the signal and LO frequencies, ν_s and ν_{LO}, respectively. The difference frequency, $\nu_{IF} = \nu_s - \nu_{LO}$, can be made arbitrarily low. The signal frequency can be downconverted into a frequency range in which low-noise amplifiers are available.

If the detector bias and preamplifier circuitry are properly designed, the system bandwidth will be limited by the extrinsic photoconductor free carrier recombination time, $\tau_r = 1/(2\pi B)$, where B is the 3-dB bandwidth. The amplitude of the detector's current response is given by

$$i_{ph} = \frac{eP}{h\nu}\left[\frac{\eta G}{1 + (\omega\tau_r)^2}\right], \tag{1a}$$

where $(eP)/(h\nu)$ is the rate at which photons of frequency ν are incident on the detector, η is the responsive quantum efficiency, and G is the photoconductive gain.[6] The photoconductive gain in turn is given by

$$G = \frac{\tau_r}{\tau_{tr}} = \tau_r\left(\frac{\mu E_b}{l}\right), \tag{1b}$$

where τ_{tr} is the mean time for carriers to transit the interelectrode distance l, μ is the drift mobility, and E_b is the dc bias field on the detector. Thus there are three fundamental material parameters that completely characterize such a detector: mobility; recombination time; and quantum efficiency.

If again the contributions due to the preamplifier and external circuitry may be neglected, the noise in the output signal is dominated by fluctuations in i_{ph} due to generation–recombination (g–r) noise, the analog of shot noise in a diode. These fluctuations are described by the relation[2]

$$\langle i_{gr}^2 \rangle = \frac{4ei_{ph}G}{1 + (\omega\tau_r)^2}\ (\mathrm{A^2/Hz}), \tag{2}$$

I. S. Park and E. E. Haller are with University of California, Lawrence Berkeley Laboratory, Berkeley, California 94720. When this work was done the other two authors were with California Institute of Technology, Physics Department, Pasadena, California 91125; E. N. Grossman is now with University of Texas, Astronomy Department.

Received 25 March 1988.
0003-6935/88/194143-08$02.00/0.

where G is the photoconductive gain. The dc (photo)-current i_{ph} is dominated by the photocurrent due to background blackbody radiation in direct detection applications and by the photocurrent due to the LO in heterodyne applications. If there is significant dark current, it also contributes shotlike noise.

Early experimental semiconductor characterization studies[7] yielded some information on carrier recombination at low temperature but were generally made in conditions quite different from those of heterodyne photomixer applications. More recent studies of high-speed photoconductors[8,9] were either concerned with response to pulsed radiation sources, in which the carrier dynamics might conceivably be different than in cw applications, or only examined a very limited number of (n-type) samples.

A substantial body of theory exists on free carrier recombination cross sections in germanium at low temperature. Recombination is an inelastic process, with most of the binding energy carried away by acoustic phonons. Because the impurity ionization energy is much greater than the energy of an acoustic phonon, $E_I \gg kT$, direct recombination into the ground state is a multiphonon process, with a correspondingly very small cross section. Therefore, the dominant process is capture into highly excited states followed by a cascade of single phonon emissions (and absorptions), as the carrier gradually diffuses into the ground state. Roughly speaking, there are two groups of theoretical work on the process of carrier recombination. The first was begun by the "giant trap" theory of Lax[10] and has since been modified and revised by many authors. Ascarelli and Rodriguez[11] developed a quantum mechanical version, and Brown and Rodriguez[12] also incorporated the phonon polarization. The second, which takes a fundamentally different approach to the problem, has been pursued by several workers and has been comprehensively reviewed by Abakumov *et al.*[13] (APY).

The Lax theory and its modifications are very complicated. They all involve a summation over the impurity's excited states of $\Sigma_{n=2}^{\infty}\sigma_n\beta_n$, where β_n is the sticking probability, the probability that an impurity in state n will eventually decay into the ground state rather than be ionized. The result of Lax's original treatment is

$$\sigma_r = \left\{\frac{\pi}{9}\left[\ln\left(\frac{\gamma}{1.78\,\delta}\right)+\frac{\delta}{\gamma}\right]\right\}\frac{1}{l_i}\left(\frac{e^2}{\epsilon kT}\right)^3\left(\frac{m^*s^2}{kT}\right)^2, \tag{3}$$

where

$$\gamma \equiv \frac{kT}{m^*s^2}.$$

Here s is the speed of sound, l_i is the mean free path for acoustic phonon scattering, and δ is a dimensionless upper cutoff to the integral for the binding energy, which must be solved numerically in terms of γ. Specifically, Lax's theory (using his quoted values for parameters such as s and m*) predicts $\sigma_r = 1.3 \times 10^{-12}$ cm^2 at 4.2 K. The results of Brown and Rodriguez cannot be expressed in an analytic form, but their numerical solution predicts a somewhat lower value, $\sigma_r = 3.5 \times 10^{-13}$ cm^2.

Abakumov *et al.*[13] state that the Lax theory and its extensions are wrong. The basic difference between APY's theory and Lax's has to do with the sticking probability at large n. Lax's theory supposes that the first capture event takes place to a level which has a binding energy of the order of kT, i.e., $n \sim 5$. APY contend, on the other hand, that at large n, σ_n increases faster than β_n decreases and, therefore, that the dominant process is recombination through very highly excited states, with binding energy $\ll kT$. APY's treatment is based on the Pitaevskii method for treating recombination in gases. Their final result is the precise analog of the Thompson cross section for recombination of electrons onto hydrogen ions, rescaled to account for dielectric screening:

$$\sigma_r = \pi r_T^2\left(\frac{r_T}{l_0}\right), \tag{4}$$

where

$$r_T = \frac{\epsilon^2}{\epsilon kT}$$

is the radius from a center at which a carrier's binding energy would be kT. Thus it is the radius at which a captured carrier has on average an even chance of staying bound. The factor r_T/l_0 is the probability that the carrier will collide with an acoustic phonon while it is within a range r_T of the center. For a capture to occur, such a collision is necessary to carry off the excess energy. Here l_0 is identified as the mean distance traversed by a carrier in one energy relaxation time, i.e., $l_0 = v_T\tau_i$. It is independent of temperature and is related to the inelastic mean free path by a factor $l_0/l_i = (kT)/2m^*s^2)$. In short, APY's theory leads to

$$\sigma_r = \frac{4\pi}{3}\frac{1}{l_0}\left(\frac{e^2}{\epsilon kT}\right)^3 = \frac{1.1\times10^{-9}}{T_K^6}\ \text{cm}^2, \tag{5}$$

where the numerical value assumes an energy relaxation length $l_0 = 4.3 \times 10^{-3}$ cm (APY 1977). The factor of 4/3 arises from a geometric average over paths within r_T of the scattering center.

The Lax and APY theories differ by a factor of approximately

$$\left(\frac{m^*e^2}{kT}\right)^2.$$

The question of the appropriate speed of sound to use is somewhat problematical, but assuming it lies somewhere between the values given by Lax for the longitudinal and transverse speeds, then

$$0.3\,K < \frac{m^*s^2}{k} < 0.8\,K.$$

APY adopt a value of 0.73 K. Thus, at 4.2 K, the recombination cross sections predicted by the two theories differ by over an order of magnitude.

Finally, we note that both theories predict a very steep increase in the recombination cross section, and, therefore, a steep increase in the bandwidth, as the

temperature is reduced. The temperature which is relevant in this case is that which describes the width of the hole distribution function T_h, which at sufficiently high bias fields can exceed the temperature of the lattice. APY predict a T_h^{-3} dependence of the cross section and, therefore, a $T_h^{-5/2}$ dependence of the bandwidth. Lax's theory predicts T_h^{-4} for the cross section at high temperatures ($\gamma/\delta \gg 1$) and T_h^{-3} at low temperatures, where the bracketed term in Eq. (3) is no longer a valid approximation. This corresponds to a bandwidth varying as $T_h^{-7/2}$ at high temperatures and $T_h^{-5/2}$ at low temperatures. Brown and Rodriguez's modification of the Lax theory predicts a somewhat gentler temperature dependence: $\sigma_r \sim T_h^{-3}$ at high T_h and $\sigma_r \sim T_h^{-2}$ at low temperature.

II. Material Preparation

Photoconductors were fabricated from a germanium single crystal which was phosphorus doped in the 5×10^{13}–1×10^{15}-cm^{-3} range. The concentration of compensating acceptors in the crystal was estimated to be 1×10^{12} cm^{-3} as determined from variable temperature Hall effect measurements. Neutron transmutation doping (NTD) was used to add further dopants to several 1-mm thick wafers of this crystal. NTD of germanium produces Ga acceptors and As and Se donors by neutron capture of Ge isotopes followed by nuclear electron capture ($^{71}Ge \rightarrow {}^{71}Ga$) or beta decay ($^{75}Ge \rightarrow {}^{75}As$, $^{77}Ge \rightarrow {}^{77}As \rightarrow {}^{77}Se$), respectively.[14] The ratio of donors to acceptors created by NTD is given by isotopic abundance and neutron capture cross sections. It leads to a compensation ratio of (As + 2Se)/Ga = 0.32.[14] All concentrations of our samples are given in Table 1. As shown, we chose three neutron fluences leading to three series of samples, each having a specific concentration of Ga and varying concentrations of compensating donors. After NTD, the Ge wafers were annealed at 400°C for 6 h in an Ar atmosphere to remove radiation damage caused mainly by fast neutrons and to activate impurities.[15] Ohmic contacts were produced by implantation with boron (1×10^{14} cm^{-2} at 25 keV and 2×10^{14} cm^{-2} at 50 keV). These implant doses lead to degenerately (i.e., metallically) doped contact areas; 200 Å of Pd and 8000 Å of Au were then sputtered on the implanted surface. The final size of the detectors was $3.0 \times 1.0 \times 0.5$ mm^3 with electrodes on opposite 1- × 3-mm^2 surfaces.

Table 1 – Doping Concentrations of Samples (cm^{-3})

Series	Sample	As grown (P)	NTD		Final	
			N_A	N_D	N_A	N_D
20	496-5.5(20)	$\sim 10^{12}$	3×10^{14}	9.6×10^{13}	3×10^{14}	9.6×10^{13}
	729-6.0(20)	5.0×10^{13}	3×10^{14}	9.6×10^{13}	3×10^{14}	1.4×10^{14}
	729-9.0(20)	8.0×10^{13}	3×10^{14}	9.6×10^{13}	3×10^{14}	1.8×10^{14}
	729-13.0(20)	1.0×10^{14}	3×10^{14}	9.6×10^{13}	3×10^{14}	2.0×10^{14}
21	729-6.4(21)	5.0×10^{13}	6×10^{14}	1.9×10^{14}	6×10^{14}	2.4×10^{14}
	729-9.4(21)	8.0×10^{13}	6×10^{14}	1.9×10^{14}	6×10^{14}	2.7×10^{14}
	729-14.6(21)	1.5×10^{14}	6×10^{14}	1.9×10^{14}	6×10^{14}	3.4×10^{14}
22	729-6.4(22)	5.0×10^{13}	1×10^{15}	3.2×10^{14}	1×10^{15}	3.7×10^{14}
	729-9.4(22)	8.0×10^{13}	1×10^{15}	3.2×10^{14}	1×10^{15}	4.0×10^{14}
	729-14.6(22)	1.5×10^{14}	1×10^{15}	3.2×10^{14}	1×10^{15}	4.7×10^{14}
	729-17.0(22)	2.0×10^{14}	1×10^{15}	3.2×10^{14}	1×10^{15}	5.2×10^{14}

III. Material Characterization

A complete characterization of the photoconductors would consist of a determination of the quantum efficiency as a function of wavelength and determinations of the recombination time and mobility as functions of bias field. These three material parameters are related to three directly observable detector properties, namely, the wavelength-dependent responsivity [defined from Eq. (1a) as i_{ph}/P], the bandwidth, and the photoconductive gain via Eqs. (1a) and (1b). For each detector characterized, we have determined the low field mobility by variable-temperature Hall effect measurements, the direct-detection responsivity at 93 and 119 μm, the bandwidth, as measured both by the frequency rolloff of g–r noise and by the frequency rolloff of response to directly modulated FIR radiation, and the photoconductive gain, as measured by the amplitude of the g–r noise. The systematic errors inherent in our experimental setup affect the accuracy of these different measurements to varying degrees, however. The nature of these systematic errors and comparison between different sets of partially redundant measurements indicate that our determinations of bandwidth are consistent and unambiguous, but that, for certain detectors, there are large discrepancies in the photoconductive gain (and, therefore, quantum efficiency) obtained by different methods.

The carrier mobility at 4.2 K was determined by variable-temperature Hall effect measurements performed on separate samples cut from the same wafers as the detectors used in the other measurements. Van der Pauw geometry was used with a sample size of $7 \times 7 \times 1$ mm^3. Ohmic contacts were prepared by boron implantation on the four corners of the sample. Because of significant hopping (dark) conductivity at the high acceptor concentrations, Hall effect measurements could not be used to determine the drift mobility in the most heavily doped samples, namely, the series 22 detectors.

Current responsivity was measured in direct (incoherent) detection at a wavelength of 93 μm (near the peak of the unstressed Ge:Ga photoconductive response) by means of a series of liquid–helium temperature filters including a narrow-bandwidth Fabry-Perot filter. The voltage-biased detector was mounted in a conventional cylindrical integrating cavity and illuminated through the cold filters by radiation from a 300-K blackbody chopped at 20 Hz against a 77-K blackbody. The total power incident on the detectors was estimated to be $\sim 10^{-13}$ W or $\sim 5 \times 10^7$ photon/s. The test system, filters, and procedures have been described previously.[16] All our detectors produced measurable amounts of dark current. For the most heavily

doped (series 22) detectors, the dark current, typically several nanoamperes depending on the precise detector and bias voltage used, was consistent with that theoretically predicted[17] for hopping conduction at the applicable acceptor and donor concentrations. Furthermore, for these detectors, it was sufficiently large that the dark current shot noise was larger than the signal current due to the $\sim 10^{-13}$ W of incident blackbody radiation. To increase the photon flux, the direct-detection responsivity was measured with the narrowband Fabry-Perot removed. The spectrum of incident radiation was now limited at long wavelengths only by the Ge:Ga photoconduction edge and at short wavelengths by the cutoff of the cold low-pass filters. This increased the flux of incident photons by a factor of 30, as measured by the photocurrent in detector 729-6.0(20), which was used for the relative calibration. Because the setup is less well characterized in this configuration and because of possible changes in the effective wavelength in this broadband mode, the 93-μm responsivities derived for the three 22 series detectors are considerably more uncertain than those of the other detectors.

The current responsivity measurements at 119 μm were made using the FIR laser described below that was used in the bandwidth and photoconductive gain measurements. The detectors were mounted at 4.2 K in similar integrating cavities of somewhat different dimensions than in the 93-μm measurements. The laser was operated on the strong 118.84-μm methanol line for all our measurements. The laser beam was focused on the input aperture of the cavity and illuminated the detector through liquid–helium temperature low-pass filters. Current–voltage curves were recorded for each detector with the laser on, laser off, and (usually) laser attenuated by various amounts as part of the setup procedure for the g–r noise measurements. The laser power was monitored from time to time by replacing the photoconductor with a pyroelectric detector. Linearity was checked by inserting attenuators into the laser beam and comparing the drop in detector photocurrent with that in the pyroelectric signal. There is a large (factor of 4) uncertainty in the absolute calibration of the pyroelectric detector, which is reflected in the absolute 119-μm responsivities derived. The uncertainty in relative responsivities, however, is limited only by laser power drifts and is much better, probably, ±25%. Comparison of the relative 119-μm responsivities with other data is difficult, however, because the 119-μm laser wavelength lies on the photoconductivity edge of Ge:Ga, whose width increases markedly with acceptor concentration due to wave function overlap. Thus the quantum efficiency is likely to vary from detector to detector much more at 119 μm than at 93 μm.

The photoconductive gain and recombination bandwidth for each detector were measured with the use of a FIR heterodyne receiver, illustrated in Fig. 1 and described in detail elsewhere.[18,19] Briefly, the system consists of a photoconductor, an 80-μm low-pass filter, and a low-noise 1–100-MHz GaAsFET amplifier

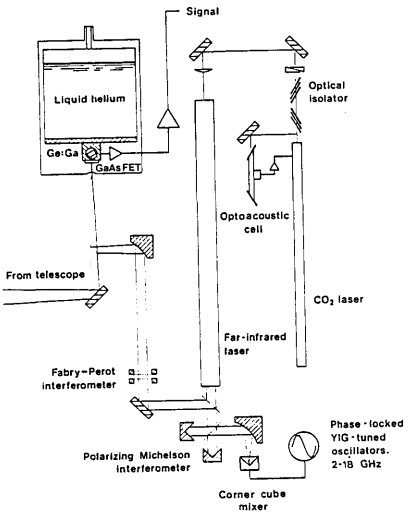

Fig. 1. Block diagram the FIR heterodyne receiver used, in modified form, to measure Ge:Ga bandwidth and photoconductive gain.[19]

mounted in a liquid–helium Dewar. Ordinarily, a FIR laser sideband generator provides a continuously tunable local oscillator for the receiver. Two techniques were used to measure detector bandwidths. The more direct one consisted of amplitude modulation of the beam of the optically pumped FIR molecular laser and measurement of the rolloff in modulated photocurrent as the modulation frequency was swept. A reflective FIR modulator was implemented by modifying the laser sideband generator shown in Fig. 1. The heart of the sideband generator is an ultralow-capacitance Schottky diode (batch 1E12, obtained from R. Mattauch's group at the University of Virginia) at the feed of a traveling-wave corner-cube antenna[20] which couples it to the incident laser beam. Modulation occurs because the traveling wave induced on the antenna is reflected off the impedance mismatch presented by the Schottky diode and reradiated. The reflection coefficient depends on the (modulated) Schottky bias voltage. Thus, for our bandwidth measurements, the 2–18-GHz YIG oscillators were replaced with a 5–100-MHz voltage-controlled oscillator (VCO), the polarizing Michelson interferometer was tuned to zero path difference, and the Fabry-Perot interferometer was removed. The same voltage ramp that was used to drive the VCO was also used to drive the internal VCO of a spectrum analyzer with which the amplified detector photocurrent was measured. Because the two VCOs were not precisely matched in linearity, the peak spectrum analyzer response would gradually drift away from the actual modulation frequency as the two were scanned, limiting the useful length of a single sweep to $\sim$45 MHz. Because the depth of modulation of the FIR laser beam was very low, due to the Schottky diode parasitics,[21] the broadband amplifier noise was not completely negligible, particularly for the high-bandwidth low-gain detectors. Therefore, a spectrum analyzer scan with the laser blocked was recorded immediately before each data scan. The digitized scans

were subtracted, and the difference was fitted to the Lorentzian spectrum of Eq. (1a).

The second technique for measuring recombination bandwidth consisted of measurement of the spectrum of the photocurrent's g–r noise. The corner-cube modulator and polarizing Michelson interferometer were removed, and the FIR laser was focused directly onto the detector cavity's entrance aperture. Spectra of the amplified photocurrent power spectrum with the laser on, attenuated by various amounts, and blocked were recorded and digitized. The conversion from noise power spectral density at the amplifier output (what the spectrum analyzer measures) and rms photocurrent is given by

$$P_{\text{out}}/B = A\left(\frac{R_d R_a}{R_d + R_a}\right)\langle i^2\rangle \text{ (W/Hz)}, \tag{6}$$

where A is the power gain of the amplifiers, B is the resolution bandwidth of the spectrum analyzer, R_a is the input impedance of the first stage preamplifier, and R_d is the differential impedance of the detector. The single-stage cryogenic GaAsFET preamplifier used in these measurements intrinsically has a very high input impedance. To improve the gain flatness, the flatness of the noise spectrum, and the system stability, its input, i.e., the IF signal line, is shunted by a resistor. When optimum noise performance is desired, the value of the resistor (which determines R_a) is about matched to R_d. For our measurements, however, the value of the resistor was set much lower, generally 200 Ω, so that RC rolloff due to amplifier input capacitance and parasitic capacitance would not contaminate the detector's intrinsic rolloff. Again a spectrum taken with the laser blocked was subtracted from each data scan, and the difference was fitted to a Lorentzian. As given by Eq. (2), the rolloff frequency yielded the carrier lifetime, and the overall power, divided by the dc photocurrent, yielded the photoconductive gain.

There are two significant sources of uncertainty in this measurement. The simplest is merely the calibration of amplifier and spectrum analyzer gains. We estimate that these uncertainties could total as much as 3 dB. They are only relevant to the determination of the photoconductive gain, of course, and not to the determination of the bandwidth. The other source of uncertianty is the sporadic existence of low-frequency (<10-MHz) noise on the laser. If it was discovered in real time, it was always found to be possible to retune the laser so as to eliminate the noise, albeit with some sacrifice in laser power. In about one-third of the measured spectra, however, an additional low-frequency component (taken to be another Lorentzian) was required to obtain an acceptable fit. In all such cases, there were spectra taken at three or more power levels so that it was possible to confirm that the excess noise component varied quadratically with laser power, as expected for laser noise. The remaining noise did fit a single Lorentzian spectrum, and scaled linearly with laser power, so we are confident it was indeed detector g–r noise. The recombination bandwidths

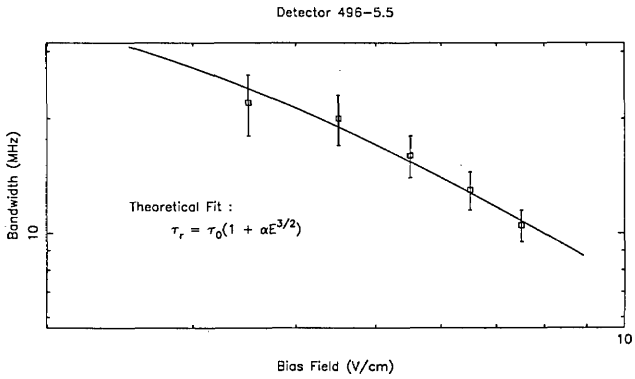

Fig. 2. Field dependence of the recombination bandwidth, measured on detector 496-5.5. The rolloff at high field is due to carrier heating.

determined by this technique agree very well with those derived by the modulation technique. The excess noise subtraction does introduce additional uncertainty into the determination of photoconductive gain (and, therefore, quantum efficiency) in those cases for which it was necessary. Together with the uncertainty introduced by the gain calibration, this renders our derived photoconductive gains considerably less reliable than our derived bandwidths.

IV. Results and Discussion

Figure 2 shows our measurements of modulation bandwidth vs bias field for a single detector, 496-5.5. The indicated error bars are somewhat conservative estimates of the range over which a good fit of the data to a single Lorentzian could be obtained. The falloff in bandwidth at high bias is due to the reduction in recombination cross section that occurs as the carrier temperature T_h is elevated above the lattice temperature.

A crude theoretical argument leads to the expectation that the recombination bandwidth should vary as $B \propto E^{-3/2}$ in the hot carrier regime and be independent of E in the thermalized regime. According to the original giant trap theory of Lax, the recombination cross section varies with mean carrier kinetic energy U as $\sigma_r \propto U^{-2} \propto T_h^{-2} \propto v_T^{-4}$ (v_T is the total mean carrier velocity). Thus the recombination bandwidth is expected to vary as

$$B = N_D \sigma_r v_T \propto N_D T_h^{-3/2}, \tag{7}$$

where $N_D = N_A^-$ is the concentration of ionized acceptors. In the thermalized (low-bias) regime, T_h is equal to the lattice temperature, independent of the field. In the hot carrier regime, the relation between v_T and bias field is given[6] by equating the rate at which energy is imparted to the carriers by the bias field with the rate at which energy is lost via inelastic (i.e., acoustic phonon) collisions. Thus

$$eEv_d = \left(\frac{1}{2} m^* v_T^2\right)\left(\frac{v_T}{l_i}\right), \tag{8}$$

where l_i is the inelastic mean free path. The drift

velocity v_d is limited by ionized impurity scattering (an elastic process) and is $\ll v_T$. It is given by the acceleration due to the field over an elastic scattering time:

$$v_d = \frac{eE}{m^*}\left(\frac{l_e}{v_T}\right). \tag{9}$$

Combining Eqs. (8) and (9), one finds $v_T \propto E^{1/2}$ or $T_h \propto E$. Thus, from Eq. (7), the theoretical expectation is thus that $B \propto E^{-3/2}$ in the hot carrier regime and is independent of E in the thermalized regime.

As shown in Fig. 2, such a dependence fits our data very well. Koenig *et al.*[7] found for much less heavily doped n-type germanium samples ($N_d \sim 10^{13}$ cm^{-3}) that $B \propto E^{-1.8}$ in the hot carrier regime was independent of E in the thermalized regime. Their lifetime measurements were made with a pulse technique, however, in which the detector slewed between conditions of impact-ionization breakdown and subbreakdown bias (the normal operating condition) at high speed. It has since been discovered that the dynamic behavior of the detectors becomes very complex near breakdown, often exhibiting high-speed spontaneous instabilities, period doubling, chaotic fluctuations, etc.[22] Thus the results of the pulsed measurements, taken in isolation, would be ambiguous. Although our measurements are in excellent agreement with the theoretical expectation deduced from Eqs. (8) and (9), they are not sufficiently accurate, or do they extend over a large enough range in bias, for us to test the dependence in great detail. We cannot distinguish between and $E^{-1.5}$ and an $E^{-1.8}$ dependence in the high bias limit, for example. Indeed, considering all the uncertainties, a bandwidth varying inversely with field is also an acceptable empirical approximation to our data over the range of practical interest, $0.5E_b < E < E_b$.

One main reason for our wanting to determine the dependence of bandwidth on bias is to be able to normalize $B(N_D)$, the bandwidth vs compensating impurity concentration, to a single value of E/E_{br}. Physically, the bandwidth in the low-bias limit, where the carriers are thermalized, would be the most fundamental quantity to examine. However, the low-bias limit is not the regime in which the photoconductors are used in practical applications, or is it a region in which we can with our techniques measure the bandwidth with any accuracy. (In both cases, the responsivity is too low.) Therefore, we have normalized all our bandwidth measurements to a bias $E = 0.8E_{br}$ using the empirical approximation of $B \propto E^{-1}$ described above. The bandwidths were actually measured at biases that varied from ~0.7 to 0.95 times the breakdown field; thus this normalization never amounted to more than an ~15% correction. The results of our measurements using both the modulation and the g–r noise techniques are displayed in Fig. 3.

These bandwidth measurements are the central result of this work. It is clear that the two techniques employed to measure the bandwidth agree fairly well. The series 22 detectors have the highest bandwidths of any we have measured—some 60 MHz measured directly corresponding to 65–70 MHz at 0.8 times the

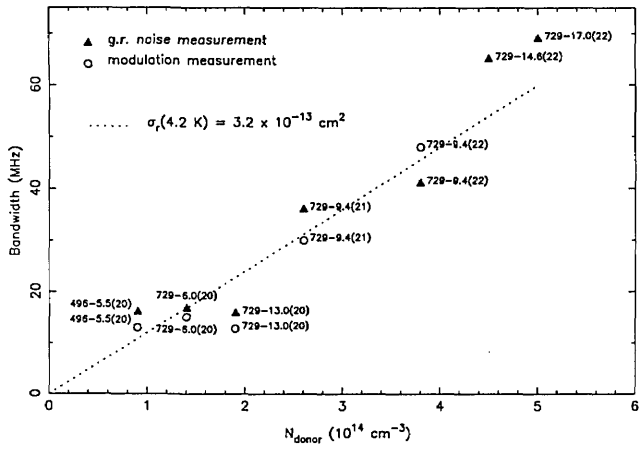

Fig. 3. Measured recombination bandwidth as a function of minority impurity concentration, for the NTD detectors. The dotted line corresponds to the linear dependence of Eq. (10) using a carrier temperature of T_h = 4.2 K and a recombination cross section of $\sigma_r = 3.2 \times 10^{-13}$ cm^2.

breakdown field. As expected from Eq. (7), there is an approximately linear relation between bandwidth and donor concentration. The slope of the relation is a measure of the recombination cross section via

$$\sigma_r = \frac{B(N_D)}{N_D v_T} = \frac{B(N_D)}{N_D}\left(\frac{3kT_h}{m^*}\right)^{-1/2}. \tag{10}$$

Taking T_h = 4.2 K we obtain $\sigma_r = 3.2 \times 10^{-13}$ cm^2. This is a slight overestimate of the cross section at the true carrier temperature [because of the $T_h^{-1/2}$ conversion factor in Eq. (10)] but an underestimate of the cross section at 4.2 K (because of the steep falloff of cross section with temperature mentioned in Sec. I). Based on the measured bias dependence of bandwidth in Fig. 2, we do not expect the bandwidth, and, therefore, σ_r, in the thermalized regime (i.e., at 4.2 K) to be more than perhaps a factor of 2 greater than our present determination, however. Compared with the theories discussed earlier, it is clear that our data favor the Brown and Rodriguez result. However, to be fair, we note that since we do not know for certain the true carrier temperature in our experiments, the extremely steep dependence of σ_r on temperature may be used to make any of the theories fit the measured cross section. For APY's theory, a carrier temperature of T_h = 15 K would have to be assumed (taking $\sigma_r \sim T_h^{-3}$), which seems implausibly high. For Lax's theory, T_h = 5.8 K (taking $\sigma_r \sim T_h^{-4}$) would suffice.

Figure 4 displays our 93- and 119-μm responsivity measurements. The plotted values were measured at slightly different biases from 0.7 to 0.9 times the breakdown field of the various respective detectors. The 93-μm measurements show a steep falloff in responsivity as N_d is increased. If η is approximately the same for all detectors at 93 μm (since this is well shortward of the photoconductive edge in germanium), this falloff reflects the decline in photoconductive gain at high compensating impurity concentrations. Such a decline is expected, partly due to the reduced recombina-

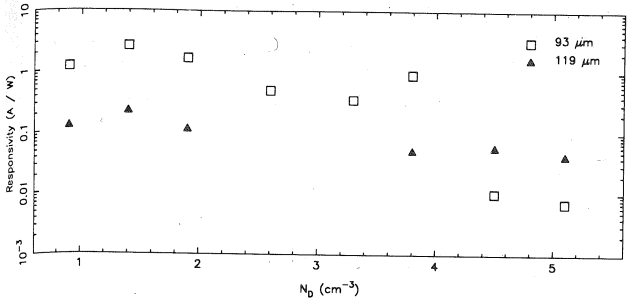

Fig. 4. Direct detection responsivity as a function of compensating impurity concentration.

tion lifetime and partly due to increased ionized impurity scattering and, therefore, reduced drift mobility. Our measured Hall mobilities indeed show such a decline, falling from 2.5×10^4 cm^2/s for detector 729-6.0(20) to 3000 cm^2/s for 729-14.6(21). The 119-μm responsivities also show a falloff at high dopings, but it is not nearly such a steep as that of the 93-μm responsivities. This may be understood in terms of impurity wave function overlap at high dopings, whose existence is implied by the existence of significant dark currents. Evidently, as the doping level is raised, the photoconductive gain falls off as indicated by the 93-μm responsivity, but an increase in quantum efficiency due to broadening of the photoconductive edge partially compensates for this, so that the falloff in 119-μm responsivity is not so steep. As mentioned earlier, the absolute value of the 119-μm responsivity is somewhat uncertain due to the pyroelectric detector's absolute calibration. The fact that some of our measurements apparently indicate $S(93\ \mu\text{m}) > S(119\ \mu\text{m})$ does not, therefore, affect this interpretation.

The photoconductive gains we have derived from the amplitude of the g–r noise are shown in Table 2. As discussed earlier, they are subject to significant uncertainties that do not affect our other data. The typical values, in the 0.01–0.03 range, are more than an order of magnitude lower than for typical detectors optimized for direct detection. In addition, there is a decline in measured photoconductive gain with increasing N_D, but it is not nearly as fast as that of the 93-μm responsivity, which, as discussed above, should track G. Indeed, the rolloff in the measured G is, at the level of uncertainty in the data, no faster than that of $S(119\ \mu\text{m})$. This discrepancy in the rate at which G and S (93 μm) decline with N_D is the basic inconsistency between our different sets of data. It depends heavily on the measured 93-μm responsivities of the two most highly doped (22 series) detectors, however. As discussed earlier, these are more uncertain than the other 93-μm responsivities because they were measured in a more poorly characterized configuration without the Fabry-Perot narrowband filter. In sum, although there is clearly a rolloff in photoconductive gain and, therefore, in responsivity, with increasing concentration of compensating impurities, our data are ambiguous regarding how fast the rolloff is.

Table 2 – Photoconductive gain derived from g-r noise

Sample	E_{bias} (V/cm)	μ_{Hall} (cm^2/V – s)	$G = \langle i^2 \rangle / 4ei_{DC}$
496-5.5(20)	5.5	-	.021
729-6.0(20)	9.8	2.5×10^4	.032
729-13.0(20)	15	9000	.028
729-9.4(21)	12	6000	.025
729-9.4(22)	18	-	.022
729-14.6(22)	20	-	.015
729-17.0(22)	25	-	.014

V. Conclusions

Ge:Ga photoconductive mixers have been developed for FIR heterodyne applications, and recombination bandwidths as high as 60 MHz have been directly measured. The dependence of bandwidth on bias field is consistent with previous measurements of very lightly doped n-type material and with theoretical expectations for the recombination cross section in the hot-carrier regime. At a given fraction of breakdown voltage (corresponding in practice to a normal operating point) the mixer bandwidth varies approximately linearly with the concentration of compensating donors. The slope of the relation yields a recombination cross section of

$$\sigma_r = 3.2 \times 10^{-13} \left(\frac{4.2K}{T_h}\right)^{1/2} \text{cm}^2.$$

This is close to the value predicted by Brown and Rodriguez's extension of Lax's giant trap theory for thermalized carriers at 4.2 K and a factor of ~30 smaller than the value predicted by APY. There is a marked rolloff in photoconductive gain at higher impurity concentrations.

These results indicate that Ge:Ga mixers can be fabricated with relatively large bandwidths. The increased bandwidth is obtained at the expense of photoconductive gain and responsivity, however. In heterodyne applications, the LO power required to obtain quantum-noise-limited performance (i.e., LO-induced g–r noise greater than other instrumental sources of noise) increases with the square of photoconductive gain. Thus increased bandwidth is obtained at the price of greater—possibly much greater—required LO power. Optimization of a heterodyne system thus involves a compromise between desired bandwidth and available LO power.

We thank J. Farmer of the University of Missouri for neutron irradiation of germanium samples. Charles H. Townes has stimulated and contributed to this work in the early stages through numerous discussions and suggestions. This work was supported in part by NASA contract W-14606 under Interagency Agreement with the Director's Office of Energy Research, Office of Health and Environmental Research, U.S. Department of Energy under contract DE-ACO3-76SF00098. Far infrared heterodyne instrumentation

research at Caltech is supported by NASA grant NAGW107.

Dan M. Watson is a Caltech R. A. Millikan fellow in physics.

I. S. Park and E. E. Haller also work in the UC-Berkeley Department of Materials Science & Mineral Engineering.

References

1. E. E. Haller, "Physics and Design of Advanced IR Bolometers and Photoconductors," Infrared Phys. **25**, 257 (1985).
2. P. R. Bratt, "Impurity Germanium and Silicon Infrared Detectors," in *Semiconductors and Semimetals, Vol. 12*, R. K. Willardson and C. A. Beer, Eds. (Academic, New York, 1977), Chap. 2.
3. A. L. Betz and J. Zmuidzinas, in presentation to L. Fisk on SOFIA (Stratospheric Observatory for Infrared Astronomy), Ames Research Center (1987).
4. H. P. Roser, R. Wattenbach, E. J. Durwen, and G. V. Schultz, "A High Resolution Heterodyne Spectrometer from 100μm to 1,000μm and the Detection of CO (J = 7–6), CO (J = 6–5), and CO (J = 3–2)," Astron. Astrophys. **165**, 287 (1986).
5. P. L. Richards and L. T. Greenberg, "Infrared Detectors for Low-Background Astronomy: Incoherent and Coherent Devices from One Micrometer to One Millimeter," in *Infrared and Millimeter Waves, Vol. 6* (Academic, New York, 1982), pp. 149–207.
6. R. M. Westervelt and S. W. Teitsworth, "Nonlinear Transient Response of Extrinsic Ge Far-Infrared Photoconductors," J. Appl. Phys. **57**, 5457 (1985).
7. S. H. Koenig, R. D. Brown, and W. Schillinger (KBS), "Electrical Conduction in n-Type Germanium at Low Temperatures," Phys. Rev. **128**, 1668 (1962).
8. F. Kohl, W. Muller, and E. Gornik, "Speed Limitation of Ge Far-Infrared Photoconductive Detectors," Infrared Phys. **18**, 697 (1978).
9. G. Dodel, J. Heppner, E. Holzhauer, and E. Gornik, "Wideband Heterodyne Detection in the Far-Infrared with Extrinsic Ge Photoconductors," J. Appl. Phys. **54**, 4254 (1983).
10. M. Lax, "Cascade Capture of Electrons in Solids," Phys. Rev. **119**, 1502 (1960).
11. G. Ascarelli and S. Rodriguez, "Recombination of Electrons and Donors in n-Type Germanium," Phys. Rev. **124**, 1321 (1961).
12. R. A. Brown and S. Rodriguez, "Low-Temperature Recombination of Electrons and Donors on n-Type Germanium and Silicon," Phys. Rev. **153**, 890 (1967).
13. V. N. Abakumov, V. I. Perel, and I. N. Yassievitch, "Capture of Carriers by Attractive Centers in Semiconductors," Sov. Phys. Semicond. **12**, 1 (1978).
14. E. E. Haller, N. P. Palaio, M. Rodder, W. L. Hansen, and E. Kreysa, "NTD Germanium: A Novel Material for Low Temperature Bolometers," in *Proceedings, Fourth International Conference on Neutron Transmutation Doping of Semiconductors*, R. D. Larabee, Ed. (Plenum, New York, 1984), pp. 21–36.
15. N. P. Palaio, M.S. Thesis, U. California, Berkeley, Lawrence Berkeley Laboratory Report LBL-16695 (1983).
16. N. M. Haegel, M.S. Thesis, U. California, Berkeley (1983).
17. B. I. Shklovskii and A. L. Efros, *1984 Electronic Properties of Doped Semiconductors* (Springer-Verlag, New York, 1984).
18. E. N. Grossman, "A Far-Infrared Heterodyne Spectrometer for Airborne Astronomy," Ph.D. Dissertation, California Institute of Technology (1987).
19. D. M. Watson, E. N. Grossman, and T. G. Phillips 1988, in preparation.
20. H. Krautle, E. Sauter, and G. V. Schultz, "Antenna Characteristics of Whisker Diodes Used as Submillimeter Receivers," Infrared Phys. **17**, 477 (1977).
21. E. N. Grossman, "The Performance of Schottky Diodes as Far-Infrared Modulators," Int. J. Infrared Millimeter Waves **8**, 1293 (1987).
22. S. W. Teitsworth and R. M. Westervelt, "Chaos and Broadband Noise in Extrinsic Photoconductors," Phys. Rev. Lett. **56**, 516 (1984).

Patents *continued from page 3952*

4,720,637 19 Jan. 1988 (Cl. 250–578)

Electro-optical imaging system and lens therefor.

P. P. CLARK. Assigned to Polaroid Corp. Filed 19 June 1986.

Although somewhat generalized, it would appear that the patent is based on the notion that an optical system relaying an image onto a 2-D detector, e.g., a CCD or vidicon, should be so designed that its image quality, or MTF, does not present spatial frequencies that are higher than the detector can faithfully reproduce. Stated otherwise, the optics act as a low-pass filter. It would seem more useful if the inventor had turned his attention to increasing the spatial frequency of the detector. R.H.

4,721,352 26 Jan. 1988 (Cl. 350–96.15)

Polarizing apparatus and method utilizing an optical fiber.

W. V. SORIN, K. LIU, and H. J. SHAW. Assigned to Board of Trustees of the Leland Stanford Junior University. Filed 27 Feb. 1986. Continuation of Ser. 833, 819, 26 Feb. 1986, abandoned.

The invention utilizes a liquid crystal to influence the light-guiding properties of an optical fiber as a function of polarization direction. The fiber is shaved and placed against the crystal material so that the evanescent field of the optical signal enters the crystal. By placing an electric field across the crystal, either plane of polarization can be reflected and preserved, or scattered and destroyed, at the interface with the crystal. R.H.

4,723,845 9 Feb. 1988 (Cl. 356–375)

Optical apparatus for the detection of position.

H. MIZUTANI and Y. SUENAGA. Assigned to Nippon Kogaku K.K. Filed 25 Sept. 1986 (in Japan 30 Sept. 1985).

This invention describes a position detection, optical apparatus engineered to obliquely project a light spot onto an object surface to be examined. The reflected light from the object surface is detected to measure the position of the surface with greater than past system accuracy. This is accomplished by projecting a light image of determined shape onto the object through a transparent plate and detecting, through the plate, the reflected light from the object on which the light image has been projected. This new system cancels aberrations that are asymmetric and generated by the transparent plate. P.M.K.

4,728,194 1 Mar. 1988 (Cl. 356–358)

Method of and apparatus for optically measuring displacement.

S. MORI, T. AKATSU, and C. MIYAZAKI. Assigned to Hitachi, Ltd. *Filed 16 Oct. 1986 (in Japan 16 Oct. 1985).*

This invention describes a method of and apparatus for optically measuring displacement of a machine requiring accurate positioning such as in a semiconductor manufacturing plant. The disclosure describes a system whereby a light beam is projected on a reference plane and on an object and the displacement of the object is measured by utilizing the interference of reflected light from the reference plane and the object to be measured. P.M.K.

4,729,620 8 Mar. 1988 (Cl. 350–96.15)

Fiber optic frequency shifter.

G. A. PAVLATH. Assigned to Litton Systems, Inc. Filed 25 May 1984.

The patent describes a method for inducing a rotating birefringence in a